AD-A160 576 A SEMIEMPIRICAL MODEL FOR DOPPLER SPECTRAL FEATURES OF MICROWAVE RADAR SEA SCATTER(U) NAVAL RESEARCH LAB WASHINGTON DC D B TRIZNA 16 OCT 85 NRL-8911 1/1

UNCLASSIFIED F/G 17/9 NL

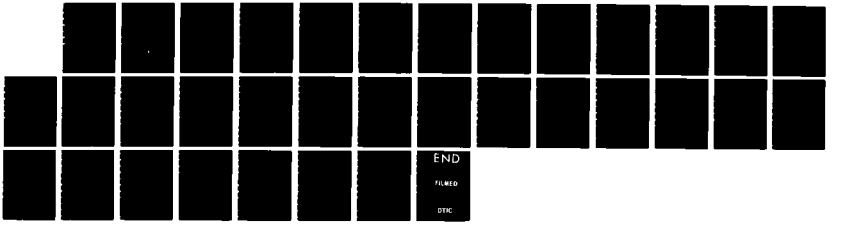

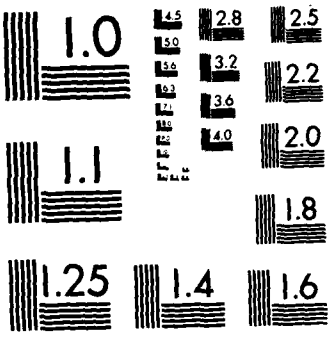

NRL Report 8911

A Semiempirical Model for Doppler Spectral Features of Microwave Radar Sea Scatter

D. B. TRIZNA

Radar Propagation Staff
Radar Division

October 16, 1985

NAVAL RESEARCH LABORATORY
Washington, D.C.

SECURITY CLASSIFICATION OF THIS PAGE

REPORT DOCUMENTATION PAGE

1a REPORT SECURITY CLASSIFICATION UNCLASSIFIED	1b RESTRICTIVE MARKINGS AD-A160576
2a SECURITY CLASSIFICATION AUTHORITY	3 DISTRIBUTION / AVAILABILITY OF REPORT
2b DECLASSIFICATION / DOWNGRADING SCHEDULE	Approved for public release; distribution unlimited.
4 PERFORMING ORGANIZATION REPORT NUMBER(S) NRL Report 8911	5 MONITORING ORGANIZATION REPORT NUMBER(S)
6a NAME OF PERFORMING ORGANIZATION Naval Research Laboratory 6b OFFICE SYMBOL (If applicable) Code 5303.1	7a NAME OF MONITORING ORGANIZATION
6c ADDRESS (City, State, and ZIP Code) Washington, DC 20375-5000	7b ADDRESS (City, State, and ZIP Code)
8a NAME OF FUNDING / SPONSORING ORGANIZATION Office of Naval Research 8b OFFICE SYMBOL (If applicable)	9 PROCUREMENT INSTRUMENT IDENTIFICATION NUMBER
8c ADDRESS (City, State, and ZIP Code) Arlington, VA 22217	10 SOURCE OF FUNDING NUMBERS PROGRAM ELEMENT NO: 61153N PROJECT NO: RR021-05-43 TASK NO: WORK UNIT ACCESSION NO: DN280-045

11 TITLE (Include Security Classification)
A Semiempirical Model for Doppler Spectral Features of Microwave Radar Sea Scatter

12 PERSONAL AUTHOR(S)
Trizna, D. B.

13a TYPE OF REPORT	13b TIME COVERED	14. DATE OF REPORT (Year, Month, Day)	15. PAGE COUNT
Interim	FROM June TO Oct 1984	1985 October 16	34

16 SUPPLEMENTARY NOTATION

17 COSATI CODES			18 SUBJECT TERMS (Continue on reverse if necessary and identify by block number)
FIELD	GROUP	SUB-GROUP	

19 ABSTRACT (Continue on reverse if necessary and identify by block number)

A semiempirical, fetch-dependent model is developed for Doppler spectral features of low grazing angle microwave radar sea scatter and is fit to data previously published in the literature. The model introduces this fetch dependence to account for the scatter in plots of the shift of the peak of the radar sea scatter Doppler spectrum data vs measured wind and surface parameters. First, constants for the model are determined by empirically curve fitting generalized versions of J. Darbyshire's fetch model equations to surface truth data (wind speed, wave height, and wave period), plotted in various combinations against one another, for 24 different experimental conditions. These constants are then applied to equations representing the Doppler shift of the peak of the sea scatter spectrum in terms of the surface truth data. Curves parametric in fetch, which are determined from these equations, are then superimposed over plots of the measured radar Doppler peak shifts vs the surface truth. It is found that these

(Continued)

20 DISTRIBUTION / AVAILABILITY OF ABSTRACT	21. ABSTRACT SECURITY CLASSIFICATION
☐ UNCLASSIFIED/UNLIMITED ☒ SAME AS RPT. ☐ DTIC USERS	UNCLASSIFIED
22a NAME OF RESPONSIBLE INDIVIDUAL Dennis B. Trizna	22b TELEPHONE (Include Area Code) (202) 767-4873 22c. OFFICE SYMBOL Code 5303.1

DD FORM 1473, 84 MAR 83 APR edition may be used until exhausted
All other editions are obsolete

SECURITY CLASSIFICATION OF THIS PAGE

19. ABSTRACT (Continues)

curves lie near the same groups of points in these plots of radar data vs surface truth, as the modified Darbyshire curves did for surface truth sets against one another. It appears that this satisfactory comparison allows one to conclude that the contributions used in modeling the Doppler shift of the radar return (large wave orbital motions, Stokes and wind drift currents, and the Bragg scatter Doppler shift) are sufficient to predict the peak Doppler shift for the vertically polarized transmit/receive combination. However, additional mechanisms are necessary to explain the larger Doppler shifts reported for the horizontal transmit/receive and the cross-polarized combinations, possibly the same that are found to produce stronger "sea spike" or "bursts" for horizontal polarizations. This has serious implications for those SAR remote sensing systems that use horizontal polarization but which use the two-scale model of radar scatter for retrieving wave information. It is to be noted that this model is not complete, in that there were no fetch measurements for comparison, but serves at this stage only to point out the importance of considering fetch as a required parameter in such modeling. A final model would require that such measurements be made.

CONTENTS

A SEMIEMPIRICAL MODEL FOR DOPPLER SPECTRAL FEATURES OF MICROWAVE RADAR SEA SCATTER

1. INTRODUCTION

Coherent radar scatter from the sea surface has two measurables of interest: backscatter signal amplitude and Doppler spectral characteristics. Several areas of application utilize these measurements. Radar scatterometry, a noncoherent measurement, attempts to correlate a large area and short time average of the backscatter amplitude of the radar return with wind speed (and possibly wave height) to allow the inference of wind stress. Determination of the probability of detection of targets in the presence of sea echo depends upon the knowledge of the short-term statistical variation of the radar return from the sea surface, termed "sea clutter" in this context. The use of synthetic aperture radar (SAR) for remotely sensing the sea surface depends upon the radar cross section spatial modulation. This includes variation across the long wave features, as well as the Doppler characteristics, but does not use an absolute measure of radar cross section.

In this report, the variation in the peak of the sea scatter Doppler spectrum is considered as a function of environmental parameters. The correlation of the Doppler spectral width with the Doppler shift presented by Pidgeon [1] can be used for a more complete characterization of the Doppler spectrum. A review of the literature on the subject of Doppler spectra, including both theoretical and experimental results, is included in Section 2. Based on these references, all the currently understood motion mechanisms that might contribute to the Doppler shift of the microwave sea scatter spectrum are identified in Section 3. An expression is developed for each mechanism in terms of the following parameters: wind speed, wave period, wave height, and the ratio of wave height to wave period.

In Section 4, radar data of Pidgeon [1] and Mel'nichuk and Chernikov [2] (henceforth referred to as M&C) are reconsidered, with regard to verification of the scattering mechanisms postulated earlier. First, scatter diagrams of measured Doppler shifts are plotted vs the derived theoretical values, which are expressed in terms of the measured ground truth data developed in Section 3. Positive correlation is found for vertical polarization (VV) that agrees with sea truth measurements made in a large number of cases. This indicates that all of the scattering mechanisms postulated are sufficient to describe the Doppler shifts for these cases. However, correlation for horizontal polarization (HH) and cross-polarization (HV/VH) with the models are not found for any case.

A generalization of Darbyshire's model for wave height and wave period as a function of wind speed and fetch is developed in Section 5. Constants for the model are determined by fitting model curves of wave height to wind speed and the wave height-wave period ratio to wind speed, using the sea truth measurements of M&C [2]. These were collected in conjunction with radar measurements of peak spectral shift of sea scatter.

In Section 6, these measured Doppler spectral peak data are plotted against wind speed, wave height, period, and ratio of height to period. For each case, a family of model curves of predicted Doppler shift is overlayed, parametric in fetch. These curves were determined from the expressions developed earlier, using constants relating wind speed, wave height, and wave period determined in Section 5.

Manuscript approved March 27, 1985.

The differential Doppler shifts are considered in Section 7; the measured Doppler shift minus the theoretical contributions are identified in Section 3. These are plotted against the wind and wave parameters, providing yet another comparison of the model with data, similar to M&C's treatment. This comparison is of much higher quality than that reported in their work, indicating the importance of considering fetch in modeling sea scatter, *via* the implicit dependence of wave height and period on this quantity. In the final section, the implications of these results are discussed, in particular in regard to applications of remote sensing of wind stress and large-scale wave structure.

2. REVIEW OF MICROWAVE DOPPLER SPECTRA RESEARCH

The Doppler characteristics of the radar return from the sea has not received much attention in the past. The only theoretical study in this area is that by Valenzuela [3], who considered the motions of Bragg scatterers in both the short gravity wave and capillary wave regions and predicted the resulting spectrum. This study did not consider the possible motions associated with the larger waves in the ocean wave spectrum, nor the effects of surface currents.

Hicks et al. [4] conducted one of the first experimental measurements of Doppler spectra of sea scatter by measuring X-band spectra from an aircraft with high spatial resolution. Because of the aircraft speed, the only reliably inferred characteristic was the Doppler bandwidth of the spectrum, for horizontally polarized radiation only. Hicks' measurements had sufficient range resolution to resolve different regions of the longest waves present and noted the effects of slightly breaking wave crests broadening the radar spectral width. This region of the wave also produced a higher shift of the spectral peak relative to those from the nonbreaking portion of the wave.

One of a series of wave tank experiments conducted by Duncan [5] at the Naval Research Laboratory provided some interesting results for both vertically and horizontally polarized radiation. Duncan et al. measured the Bragg line returns from capillary and short gravity waves for several depression angles and described the behavior as the longer wave portion of the spectrum became excited. However, these measurements were for very modest winds and fetches and were conducted for the purpose of understanding the fundamentals of the scattering process, not for duplicating the more complicated motions which occur under open ocean conditions.

Pidgeon [1] performed the first radar Doppler measurements of sea scatter from a stable platform on land at two different sites, using a C-band radar with both horizontal and vertical polarizations. At the first site, in Puerto Rico, a spar buoy was used for measuring the wave height, wind speed and direction, and other meteorological parameters. At the second site, the radar was used for measuring the ocean wave lengths and wave speeds, and the wave heights were inferred from these by using a wave growth model. (At the second site, the wind measurement location was not specified, but if made at the radar site located on a 50 m bluff, these could be strongly affected by the land contour.) Both sets of data were mixed in the reporting, and one cannot separate the effects of these differences in ground truth between the two sites.

Independent of any ground truth comparisons, however, Pidgeon reported some interesting results. First, he showed that the Doppler bandwidth of the radar return scales linearly with Doppler shift of the spectrum peak. The slope for horizontal polarization, 0.571, is half the value measured for vertical polarization, 1.143. Second, for depression angles between 0.5 and 3.5 deg, both the Doppler bandwidth and the peak shift are essentially independent of depression angle. Third, the Doppler shift of the peak varied as the cosine of the angle to the wind, whereas the Doppler bandwidth remained constant with this angle. Fourth, his Doppler shift measurements for vertical polarization were fit as a function of wave height to a curve which indicated that the orbital wave motions were the sole cause of the shift, a point discussed later. Fifth, for the horizontally polarized data, he plotted a differential velocity, the peak Doppler shift minus the orbital velocity, vs wind speed. He then empirically fit a

curve to this data, apparently assuming that the orbital velocity dominates the peak Doppler shift, which is not necessarily the case.

The final report on Doppler characteristics of radar sea scatter is that by M&C [2]. Their sea truth consisted of measurements of wind speed, wave height, and wave period made 10 km from the radar measurements by an oceanographic vessel, and they report both sea truth and radar data in tabular form for each of 24 experiments. They used an X-band radar with both horizontal and vertical polarization and reported on peak Doppler shift vs wind speed, as well as on a different differential velocity: measured spectral peak Doppler shift minus orbital motion and wind drift contributions. Although wave height and periods were measured, these were not compared with radar measurements. They fit a straight line to all observations for both cases, observed a relatively broad spread in the data for the HH, VV, and HV combinations, and they concluded that not all contributions to the Doppler shift are accounted for by the two-scale model first suggested by Wright [6] and others.

M&C also measured the azimuthal dependence of the peak Doppler shift and found a cosine dependence, similar to that found by Pidgeon. They studied the variation of the peak Doppler shift for short fetches between 1.1 and 9 km for offshore winds, using sea truth derived from an empirical model of Darbyshire [7], and again concluded that the two-scale model is not sufficient to explain these short fetch observations.

These results appear to be the most comprehensive of all those discussed here, and they form the basis of what appears in the remainder of the report. Because they report measurements of wind speed, wave height, and wave period for all radar experiments conducted, the various contributions to the Doppler spectral shift can be calculated from theoretical considerations, and compared with the actual measurements on a scatter diagram. This is described in the following two sections.

3. MODELING THE SOURCES OF PEAK DOPPLER SHIFT

In this section, the Doppler shift of the peak of the sea scatter Doppler spectrum is modeled for very low grazing angles, in a manner similar to that of M&C. Although this Doppler shift model is also based on the two-scale model for radar scatter [6], it differs from M&C in two respects. First, additional motions beyond the orbital wave motions and wind drift are included, namely, Bragg scatterer phase velocity and Stokes drift currents. Second, the period of the peak of the ocean wave spectrum is used to parameterize vs radar data rather than their average wave period. M&C used this parameter, assuming all ocean wave components were illuminated with equal probability, not taking into account wave shadowing at low grazing angles. In addition, a modified form of the orbital wave velocity first applied by Pidgeon to radar data is shown to be equivalent to Stokes wave corrections to the linear theory and is thus included in the model implicitly. An increasingly better fit of model curves to radar data is observed as each addition to their model is employed in successive versions.

The argument for using the peak of the wave spectrum for parameterization against radar data is as follows. Because of severe shadowing which occurs for low grazing angles, the main surface scattering contribution will come from the region about the crests of waves, and in particular, the crests of the highest waves. That is, the highest waves are not only responsible for the shadowing of smaller waves but are also preferentially illuminated as a result of the shadowing process. Hence, with the added assumption that the backscattered power is dominated by these preferentially illuminated waves, it follows that the orbital wave motions of the highest waves will provide the dominant contribution to the Doppler shift. (An estimate of the absolute amplitude of this contribution would require consideration of the statistics of wave heights and is beyond the scope of this work.) Accepting any one of many models for the ocean wave spectrum, the highest waves will generally also correspond to the longest waves present in the wind-driven portion of the ocean wave spectrum. (See, for example, Phillips [8].) Although the highest wave features are in fact the sum of several different wave spectral components,

statistically the longest wave components will to a high degree of probability contribute to the highest wave features observed. This assumption of the longest waves providing the largest backscatter amplitude contribution to the Doppler spectrum thus suggests use of the period of the peak of the measured wave spectrum reported in M&C as a variable against which to parameterize, rather than the mean wave period which they used, taken as 0.77 times the period of the ocean wave spectral peak. Expressions for each of the contributions to the Doppler shift of the peak of the spectrum are derived in the remainder of this section.

a. Bragg Scatterer Phase Velocity

According to the two-scale model, radar sea scatter is produced by the Bragg scatter from ocean wave components satisfying the Bragg scatter relationship [9]:

$$K = 2k \cos \phi , \tag{1}$$

where K is the ocean wave number, k is the radar wave number, and ϕ is the grazing angle of the radar wave measured relative to the horizontal. For microwave frequencies, these wavelengths lie typically in the capillary to short gravity wave region, and for X-band frequencies in particular, they lie midway between these two regions. This midpoint is determined by Phillips [8] as that wave frequency for which the gravity wave and capillary wave contributions to the phase velocity of the wave are equal. This phase velocity is calculated by using the dispersion relation for deep water waves:

$$\Omega^2 = gK + K^3 \tau / \rho \tag{2}$$

where g is the acceleration of gravity, τ is the surface tension, ρ is the density of water, and Ω is the ocean wave frequency. The phase velocity Ω / K has a minimum at this point, 23 cm/s, for a water wavelength of 1.7 cm, and is independent of wind speed. The Bragg resonant wavelength for near zero grazing angle from Eq. (1) is 1.6 cm for an X-band radar (9.4 GHz), with a phase velocity of 24 cm/s, which is very close to this minimum phase velocity.

b. Orbital Wave Velocity Contributions

The short Bragg-resonant scatterering elements of the previous section are moved about by the motions of the long waves: for small to moderate wave heights, a point on the sea surface moves in a circular orbit as a large wave passes by. Under these conditions, the linear approximation is satisfactory for the equations of motion of particles on the wave, and the wave profile is approximated as sinusoidal. The orbital wave velocities are given by simple harmonic motion:

$$V_0 = \Omega \ H/2 = \pi \ H/T \tag{3}$$

where Ω is the radian frequency of the long gravity wave (of period T), and H is its height from crest to trough.

In his analysis, Pidgeon used a modified form of the orbital wave velocity, from an empirical study by Mee [10] conducted in a wave tank. This contribution is considered in this work as well. Because Mee's results can be described equivalently by Stokes drift currents, they are treated in the next section.

c. Stokes Drift Currents

As waves begin to achieve relatively high ratios of wave height to wavelength, their shapes become more trochoidal rather than sinusoidal, and the Stokes solution to the equations of motion for gravity waves must be used (see, for example, Kinsman [11, pp. 254-258]). As a result, the water particle motions are no longer closed orbits, but the particles slowly advance with a cycloidal type of movement with the direction of the advance that of the primary wave energy.

The effective average current which results is a function of depth, as shown in Kinsman [11, pp. 504-510]). The drift current at depth z is given by the following equation for a closed system, such as a wave tank:

$$V_{SD} = \Omega\ K(H/2)^2\ [\cosh 2K(z + d)/(2 \sinh^2 Kd)] - (\Omega(H/2)^2/2d) \coth Kd \tag{4}$$

where d is the depth of the water. The second term of Eq. (4) is a result of requiring the total mass transport to be conserved, as in a wave tank, resulting in return flow beneath the surface. For open ocean conditions, this requirement is not met, and this term is taken to be zero, as it was a constant of integration determined by the specified boundary conditions. For very deep water and at the surface, where $z = 0$, the first term of Eq. (4) reduces to:

$$V_{SD} = 2\pi^3\ (H/T)^2/gT\,. \tag{5}$$

Although Mee's original work is not readily available, and the depth of his tank not known, as noted in Pidgeon, Mee found that his measured values of the orbital wave velocity varied from the predicted by Eq. (3) for large wave height to wavelength ratios. His results were fitted according to the following empirical formula:

$$V_0 = \frac{\pi\ H/T\ \{1 - \delta \cos \psi\}}{\{1 + \pi\ H/L \cos \psi\}} \tag{6}$$

where π is the phase of the position on the long wave measured relative to the trough, L is its wavelength, and δ is a function of wave height and the intensity of whitecapping. For motions at the crests, which provide the greatest Doppler shift, $\psi = \pi$ and $\cos \psi = -1$. For the low grazing angle case, as noted above, the scattering elements located near the crest will be preferentially illuminated, so that these values are used in the model. The quantity δ was shown by Mee to be small, and it is neglected in this treatment. Thus, by using the dispersion relation of Eq. (2), with only the gravity wave term retained, and solving for $1/L$, Eq. (6) is rewritten as:

$$V_0 = \frac{\pi\ H/T}{\{1 - 2\pi^2 H(gT^2)\}}. \tag{6a}$$

The second term in the denominator is small for all physically realizable waves, and the denominator can be expanded in a Taylor series and yields to second order in H/T:

$$V_0 = \pi H/T\ \{1 + 2\pi^2 H/(gT^2)\}\,. \tag{6b}$$

This expression is just tne sum of the classical orbital wave velocity and the Stokes drift contribution of Eq. (5). One can infer that the measurements of Mee were thus made in relatively deep water for the wavelengths generated, such that the second term of Eq. (4) was insignificant.

d. Wind Drift

The final contribution to consider is that due to wind drift. This results from the continuity of stress across the sea surface as momentum is transferred from wind to waves. The wind speed at the sea surface is extremely difficult to measure, and it can only be inferred by using models for atmospheric convection. The atmosphere is said to be neutral, stable, or unstable toward convection if a parcel of moist air remains at the same altitude, falls, or rises when it is displaced vertically from some initial point (see, for example, Kraus [12]). For altitudes much higher than the crests of the tallest waves, the wind profile for neutral buoyancy satisfies a logarithmic behavior with altitude. For stable or unstable conditions, a correction factor to this profile is defined which is a function of the roughness length of the surface and atmospheric stability. The literature has no data that can be used to determine the wind drift of the water surface as a function of atmospheric stability, but only results which indicate that this drift is about 3% of the wind speed at 10 m. Since M&C reported neither the height of the wind measurement nor a stability parameter, we assume a 3% value in this work. Since the contribution of the wind drift is small relative to the orbital velocity and Bragg contributions, the error due

to this assumption is not expected to be a large one except at very high wind speeds beyond those reported in M&C. The expression for the wind drift current used in this work is thus taken to be:

$$V_{WD} = 0.03\ V_W. \tag{7}$$

4. TESTING THE SPECTRAL PEAK DOPPLER SHIFT MODEL

With each of the four contributions to the Doppler shift expressed as a function of the sea truth parameters reported by M&C, the accuracy of different versions of the Doppler model can be tested by comparing each version with the radar data in M&C. All measured Doppler shifts were reported for depression angles ranging from 0.1 to 2.0 deg, for 24 different experiments. Their experimental results yielded no differences in Doppler shifts over this range of angles for a given set of sea conditions.

The first test of the set of models is a scatter diagram of M&C's measured Doppler shifts vs the modeled values, which are expressed in terms of their measured sea truth parameters. Three different versions of the model are calculated. The first is most similar to that of M&C, using the traditional expression for the orbital wave velocity and M&C's "average" wave frequency, but adding the Bragg phase velocity, 24 cm/s. The second version of the model includes the Stokes current contribution given in Eq. (5) (equivalent to the modified orbital velocity of Eq. (6b)), along with the average wave frequency. The final version used adds the use of the peak ocean wave frequency in the expressions for the Doppler velocity contributions. Table 1 summarizes the three different models.

Table 1 — Expressions and Parameters Used in the Models

Model Number	Parameterized Wave Frequency	Orbital Wave Velocity	Bragg Scatter Phase Velocity (cm/s)
1	$0.77 * T_{peak}$	Equation (3)	24
2	$0.77 * T_{peak}$	Equation (6b)	24
3	T_{peak}	Equation (6b)	24

In the plots, the spread in the data about a straight line is assumed to be due to either experimental error or the inherent variance of the sea surface. The criterion used in the test of each model will be how close the data fit a straight line of slope one. A least squares fit to the data is not performed because it was shown elsewhere [6] that fetch effects will also cause a spread in the data, and that the straight line of unit slope should be approached asymptotically only for fully developed waves.

Figure 1(a) is a plot of the measured Doppler shifts for vertical polarization, using version one of the model. The apparent slope of the data is greater than the expected value of unity, indicating less than perfect correlation of the data with the model. The data lie slightly nearer to the unit slope line in the scatter diagram of Fig. 1(b), using the second version of the model, indicating that addition of the Stokes currents offer a significant improvement over the M&C model. Finally, Fig. 1(c) shows the result of use of the third model. A larger shift in the data to the unit slope line than was achieved in the second model is seen here, indicating the shadowing effect is larger than Stokes second order contribution for the range of surface truth reported in M&C.

As the radar depression angle is increased to values much larger than zero and shorter gravity waves are no longer shadowed by the longest waves, one would expect to see a broadening of the sea

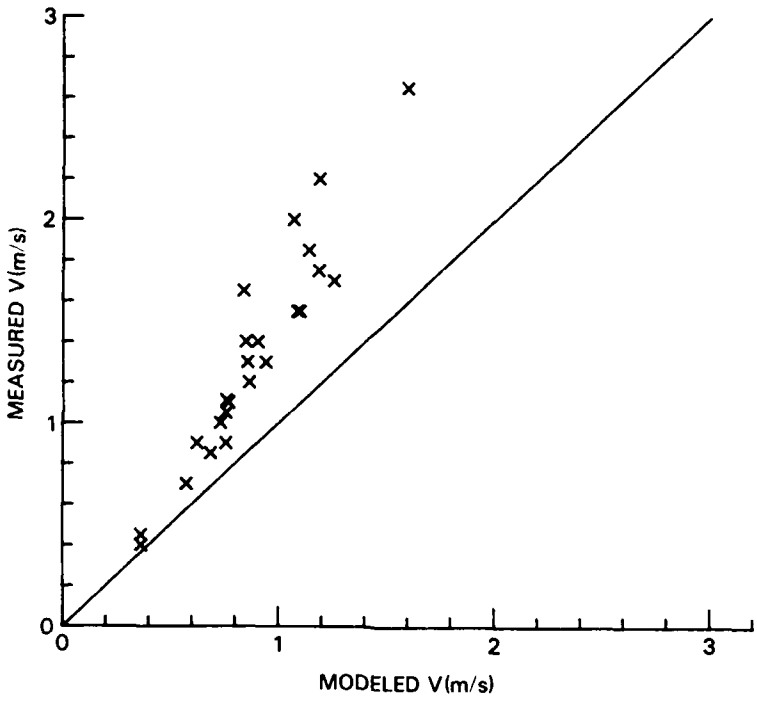

Fig. 1a — Measured peak Doppler shift of the sea scatter Doppler spectrum for vertical polarization vs the sources of Doppler shift modeled in Section 3, expressed in terms of measured values of wind speed and wave height and "mean wave period," reported by Mel'nichuk and Chernikov. The familiar expression for the orbital wave velocity of Eq. (3) was used to model this contribution to the Doppler shift.

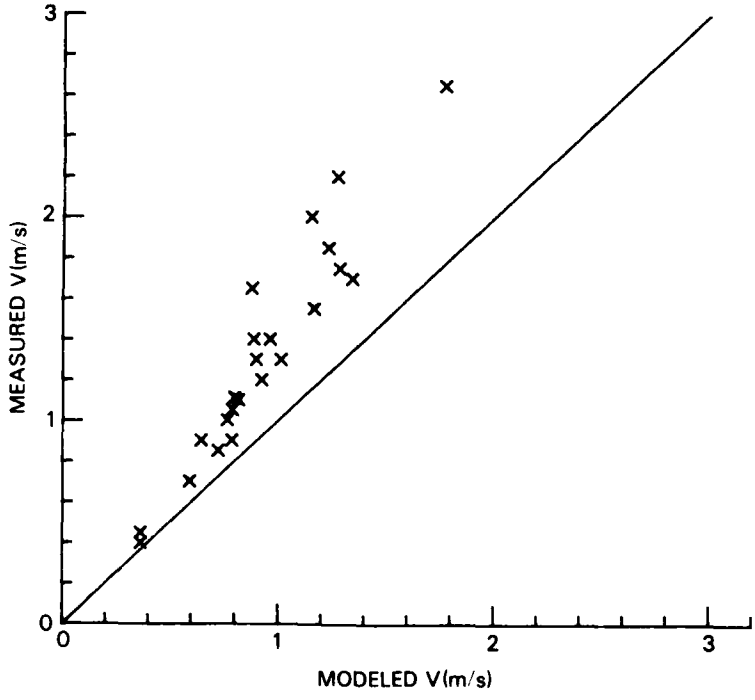

Fig. 1b — A scatter diagram similar to Fig. 1a, but using the expression in Eq. (6b) for the orbital wave velocity contribution to the Doppler shift

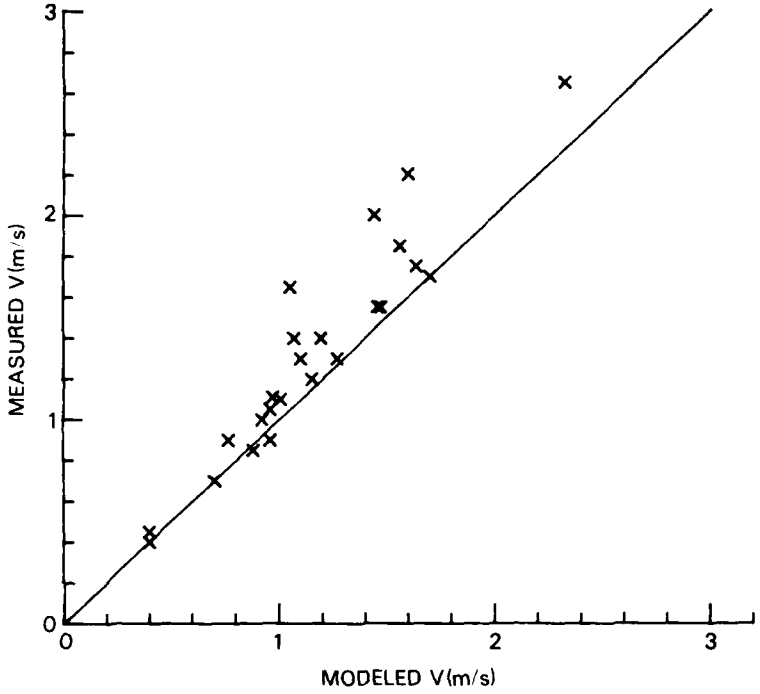

Fig. 1c — A scatter diagram similar to the previous two figures, but using Eq. (6b) and using the measured frequency of the peak of the wave spectrum in all expressions for the modeled Doppler shift, rather than the mean value used by Mel'nichuk and Chernikov

scatter Doppler spectrum toward smaller values of Doppler frequency if the shadowing concept presented here is correct. The mean frequency of the wave spectrum might be a more realistic value to use in that case, although this would require a more detailed analysis of the scattering contribution associated with each surface wave component illuminated.

The result of plotting the horizontally polarized and the cross-polarized data with the same method as is used in Fig. 1c is shown in Figs. 2 and 3, respectively. A much poorer scatter diagram fit to a unit slope is obtained. This is an indication that there are additional scattering mechanisms with associated Doppler contributions which have not yet been identified for these two cases. If one plots the measured horizontal vs the measured vertical Doppler shift, and then the measured cross-polarized data vs the vertically polarized, Figs. 4 and 5 result. The very narrow scatter in the data along the linear curves is an indication that the unidentified Doppler shift mechanisms for these two cases scale in the same way with the environmental parameters as do the Doppler shift mechanisms for vertical polarization.

With this implicit verification of the model for the spectral peak Doppler shift contributions for vertical polarization, we now attempt to utilize this model to investigate the fetch dependence of the peak Doppler shift as a function of the measured environmental parameters, and see if a definite correlation can be found.

5. FETCH-DEPENDENT MODEL FOR ENVIRONMENTAL DATA

This section considers the sea truth data of M&C: wave height H; period T; wind speed V; and the ratio of wave height to period, H/T. We attempt to identify trends in plots of wave parameters vs

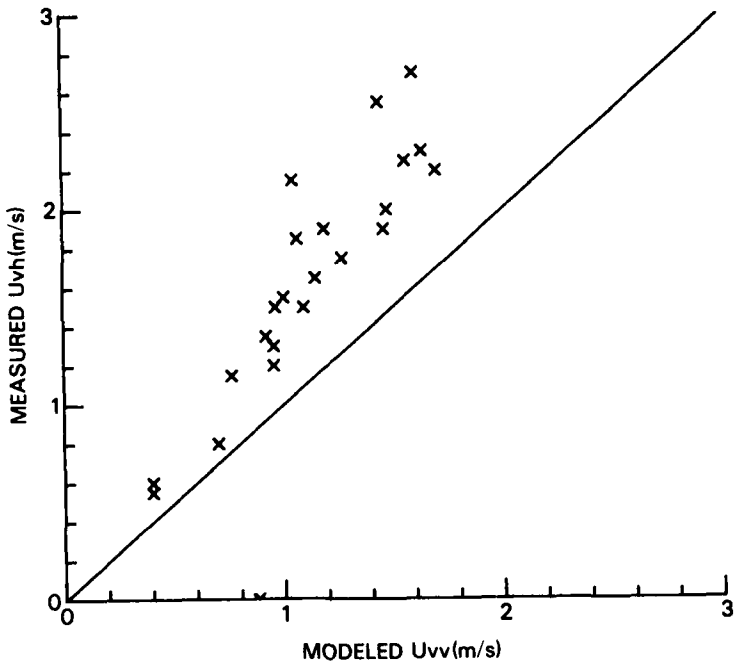

Fig. 2 — A scatter diagram similar to that in Fig. 1c, but for the cross-polarized radar return (horizontal transmit and vertical receive or vice versa)

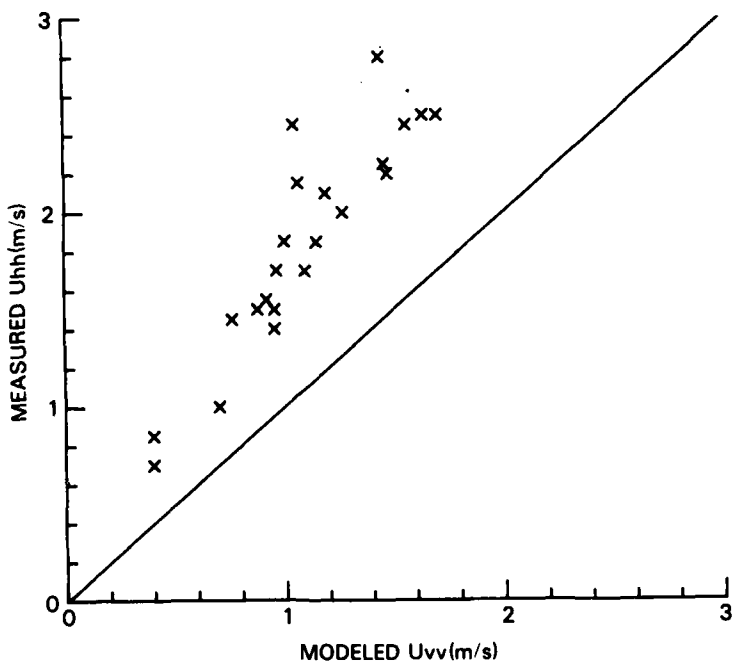

Fig. 3 — A scatter diagram similar to that in Fig. 2, but for the horizontally polarized radar return.

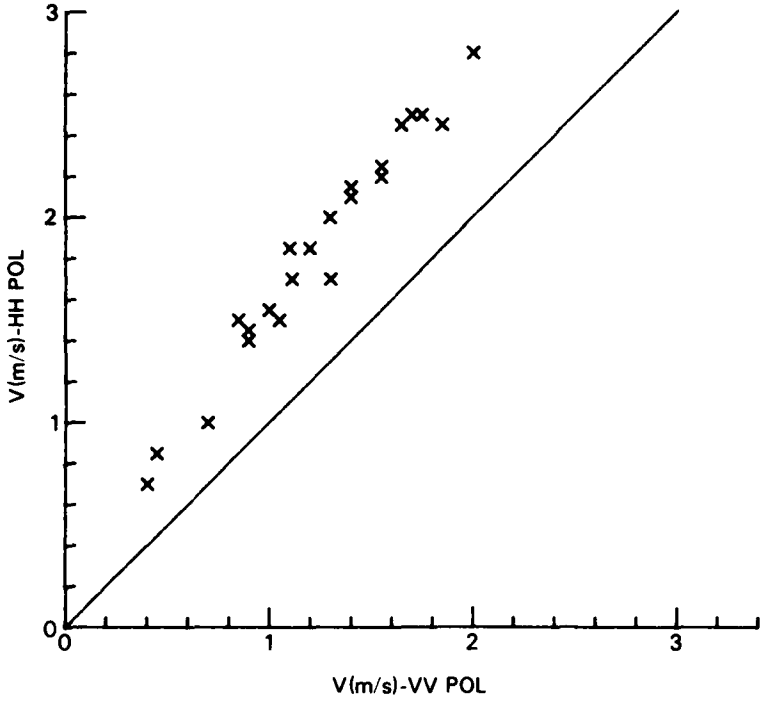

Fig. 4 — Measured Doppler shifts for horizontally polarized return vs that for the vertically polarized return

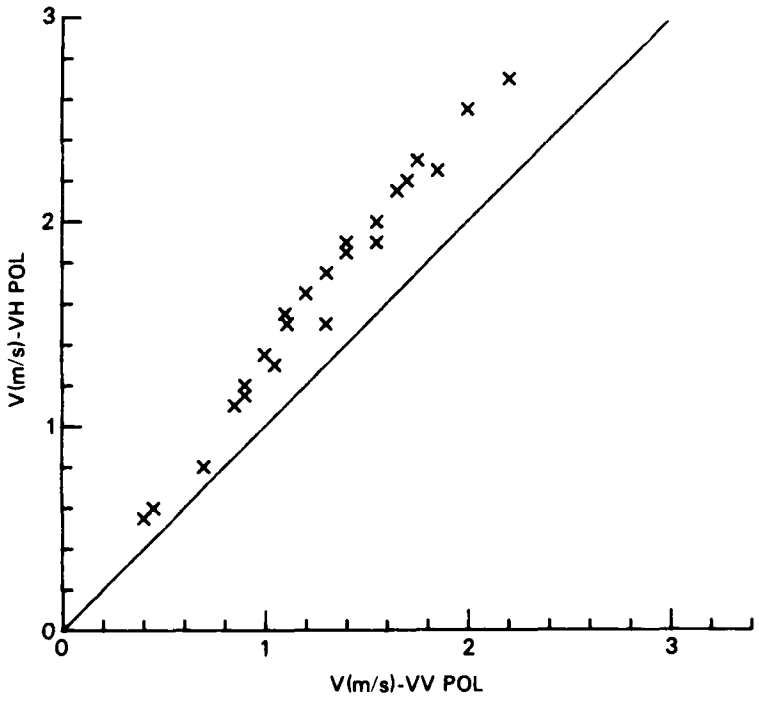

Fig. 5 — A scatter diagram similar to that in Fig. 4, but for cross-polarized return vs the vertically polarized return

wind speed. A family of parametric curves is generated by using an extension of Darbyshire's empirical fetch model [7] and overlayed upon these plots, with model constants chosen to provide a subjective fit to the data. These model constants are used in the next section with the model curves for radar Doppler shift of the sea scatter spectral peak.

Modification of Darbyshire's Model

Darbyshire's original model [7] referenced in M&C was derived empirically, based upon a data set for fetches up to 18 km and wind speeds from 4 to 9 m/s. The data were presumably not duration-limited for these relatively low values. However, the data which we consider include wave periods ranging from 0.235 to 0.5 Hz, and wind speeds as high as 12 m/s. According to Fig. 8.4-5 of Kinsman [11], these waves require far less than a 4-h duration to be fetch-limited rather than duration-limited. Since no model exists that expresses wave height and period in terms of both fetch and duration limitations, we assume that the waves were not duration-limited and use Darbyshire's model. We are not attempting to develop a rigorous fetch model at this time, since no fetch measurements were made. We are simply attempting to illustrate that the scatter in the radar data reported in M&C is due to fetch variation in conjuction with our earlier demonstration that the two-scale model appropriately describes their data for vertical polarization.

Darbyshire's model for wave height and period in terms of wind speed is given in general form by:

$$H = 0.0153 H_m \; Y^{H_p} \; V^2 \tag{9}$$

and

$$T = 2.7 T_m \; Y^{T_p} \; V^{1/2}, \tag{10}$$

where

$$Y = (X^3 + 5.6X^2 + 222X)/(X^3 + 22.2X^2 + 888X + 5.4) \tag{11}$$

with X being the fetch in kilometers, and where T_m, T_p, H_m, and H_p are model fitting constants. H_m and T_m are equal to one in Darbyshire's model, and we effectively scale relative to his constants, 0.0153 and 2.7. His original empirical model was not sufficient for our purposes because the ratio H/T did not vary with wind speed as did H and T, thus requiring including the added coefficients, H_p and T_p. The strategy was to choose that set of coefficients for which H and H/T vs wind speed fit the data in a similar fashion, i.e., curves for a given fetch overlayed the same groups of data points.

Other experiments have required different coefficients than Darbyshire's to fit their data as well. Sverdrup and Munk [13] have observed values of H_m as large as 1.75, as shown in Kinsman [11, p. 391], with the error in his ordinate plot labels corrected by multiplying by 10, and the constants corrected by multiplying by 100, for wave height in units of meters.

If one forms the ratio of H/T in the above equations, one sees that the dependence on Y vanishes for Darbyshire's original choice of constants:

$$H/T = 0.00567 \; V^{1.5} \tag{12}$$

so that all data points should lie on a single line. However, when the data of M&C are plotted as H/T vs V, they do not fall along a single curve, but exhibit a spread. Also, individual points are found to lie in groupings similar to the plots of H vs V and T vs V, as seen by comparing Figs. 6, 7, and 8. The assumption is that this same sense of spread in H/T is due to a fetch-dependence as well, and the constants T_p and H_p were introduced to allow for this, giving a more general form of Eq. (12):

$$H/T = 0.00567 (H_m/T_m) \; Y^{(H_p - T_p)} \; V^{1.5}.$$

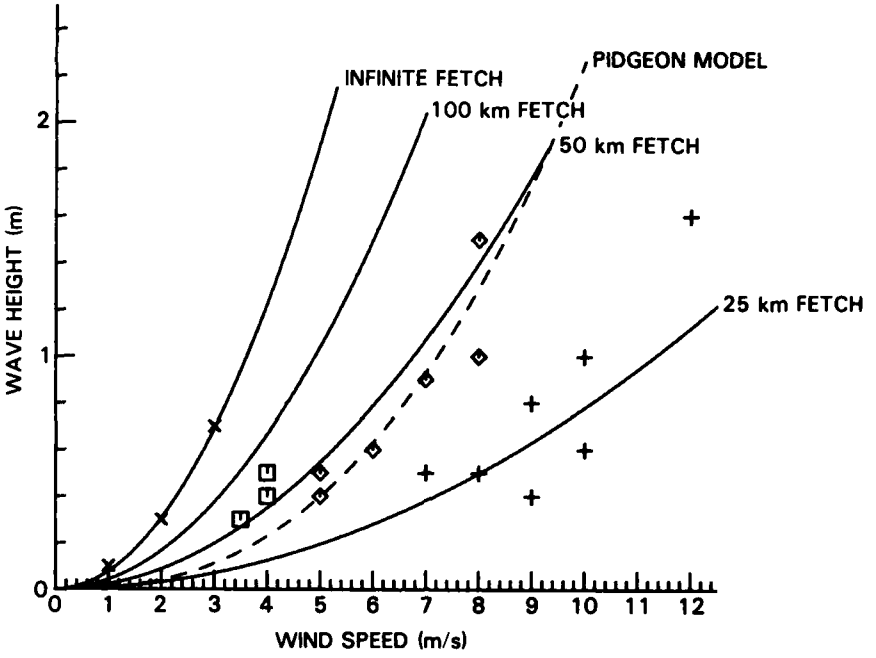

Fig. 6 — Surface truth data reported by Mel'nichuk and Chernikov of wave height vs wind speed are plotted. Curves are overlayed which are calculated from Eq. (12) in the text, with values of the constants $H_p = 3$ and $H_m = 5$ used.

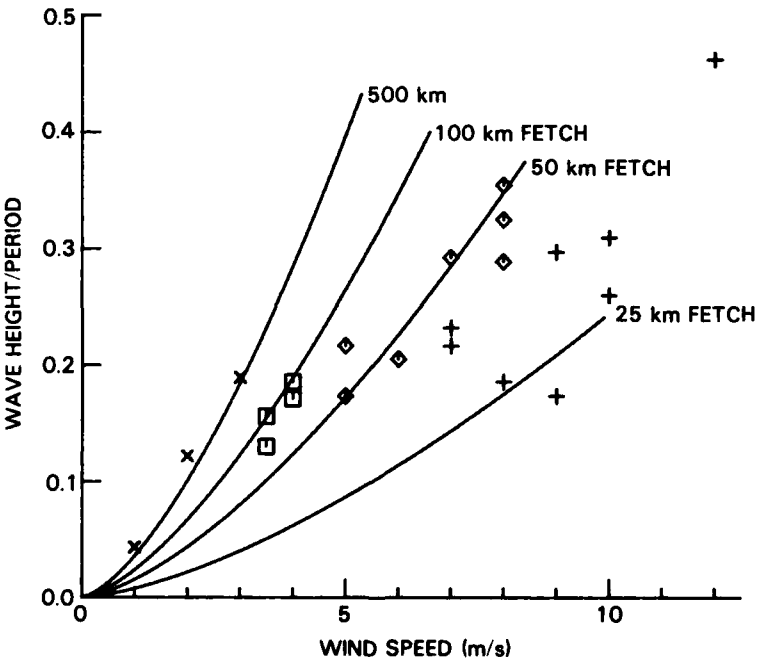

Fig. 7 — Plots similar to those in Fig. 6a, but plotting the ratio of wave height over wave period vs wind speed. Curves were generated using both Eqs. (9) and (10) in this case, for constants $H_p = 3$, $H_m = 4$, $T_p = 1$, and $T_m = 0.8$.

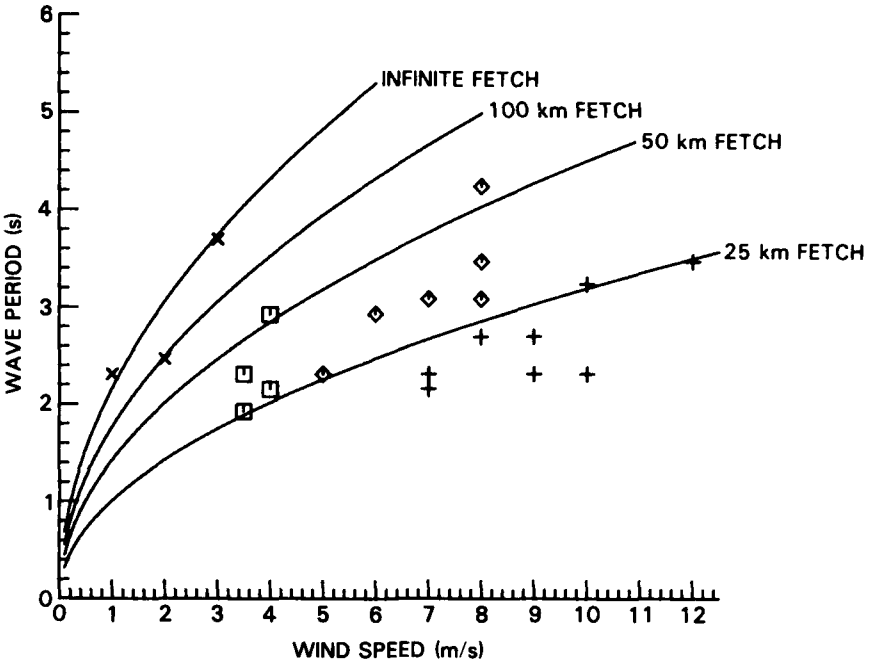

Fig. 8 — Plots similar to those in Fig. 7, using the same constants, but of wave period vs wind speed. The constants were chosen using the data combinations of the last two sets of figures, and the curves for this plot are fixed by that choice.

The choice of $H_p > T_p$ was made to let H grow faster than T with fetch in our model because of the observed sense of spreading of the H/T data, as shown. This also agrees with similar observations that wave heights grow faster for conditions of unstable atmospheric conditions than for stable conditions (see, for example, Liu and Ross [14]).

The data we are considering were collected with onshore winds, since offshore wind data were treated separately in the section on the very short fetch study conducted in M&C. (There they used fetches between 1 and 10 km, and showed only a marginal fetch-dependence, as would be expected by our curves for such small fetch values.) In all of the above, no swell contributions were considered, as there were none reported by M&C. Since the location of the radar experiments was not given, it is not known if swell was present.

Fitting of the Model Curves

The results of plotting the wave height vs wind speed are shown in Fig. 6, for values of $H_p = 3$ and $H_m = 5.0$. The multiplicative constant, H_m, raises the family of curves with increasing value, and this value was required to fit the lowest wind speed data. The exponential constant, H_p, spreads the family downward, but does not affect the highest curve, for which $Y = 1$ and therefore exhibits no dependence on fetch, X. This value of H_m required to fit the highest fetch data is larger than the 1 of Darbyshire [7] and 1.75 of Sverdurp and Munk [13]. The value of H_p used to fit the right-most data group to a 25-km curve is arbitrary in the sense that no fetch measurements were reported for these observations against which to compare. We chose 25 as the minimum value since offshore winds might be expected to have a fetch determined by the scale size of a weather system, rather than another coastline. A larger value of H_p would pull the 25-km curve to a lower wave height region for the same wind speed.

The fitting of the family of curves was done as follows: first, the choice of $H_m = 5$ was made to fit three data points marked by a cross, "X," as fully developed waves in Fig. 6. There are actually five data points here, with two pairs identical. A similar fit to points representing these experimental periods was done in a plot of H/T vs wind speed shown in Fig. 7, in which T_m was varied until the infinite fetch curve passed through the data in question.

T_p was chosen to be one, in agreement with Darbyshire. We have the freedom to modify this constant if necessary because we have overspecified the set of equations until we have fetch information available. The exponential constant H_p was then chosen to provide a reasonable fetch to fit the data points marked with "+" in both figures, with the *caveat* repeated that this was done for illustrative purposes only, since fetch measurements were not available for comparison. The remainder of the data were labeled according to the nearest fetch family curve. H/T was used rather than T for model fitting because this ratio is a dominant term in the orbital wave velocity contribution to the Doppler shift.

The plot of H/T is shown in Fig. 7. Had the difference in Eq. (11), $H_p - T_p$, been negative, the family of curves would have spread in the opposite direction; i.e., the same infinite fetch curve with $Y = 1$ would have been the lowest of the set. Hence, because the data points lie relative to one another as they do, we can conclude that the difference in constants is of the correct sign with the choice made here.

Figure 8 shows the results of the choice of T_p and T_m on the plot of T vs V. The curves show similar trends for the very long fetch data, and the shortest fetch data lie near the 25-km curves again, showing reasonable internal consistency, as they should. That is, the curves that fit this data set are not independent of the H/T data for which the curve fitting was performed.

Although the set of constants was chosen in a physically reasonable way, it must be reiterated that there is no guarantee that the curves shown are correct since no fetch measurements were made for comparison. The most we can say is that the scaling is probably correct from one plot to another among the different fetch curves plotted, but that the explicit value of the fetch must await confirmation by further experiments. The important point to note for later comparison with radar data is that, once a set of symbols were assigned to each data set based upon their ordering in the H vs V plot, these points continued to show the same ordering over the three different wave parameters when fitted against wind speed. The next step is to plot the radar data in similar fashion vs wind speed and other wave parameters and consider their spread.

6. DOPPLER SPECTRAL SHIFT VS ENVIRONMENTAL PARAMETERS

The constants used to fit the environmental data of the last section are now used to define a model for Doppler shift of the spectral peak of the radar sea echo spectrum, parametric in fetch. Spectral shifts of the peak of the sea scatter Doppler spectrum are predicted as a function of the various sea truth measurements, with fetch as a parameter of the model. The model is presented as a family of theoretical curves, each curve corresponding to a given fetch value. These curves are plotted to overlay the plots of radar data vs the sea truth parameters. First, the peak Doppler shift for vertical polarization is considered, as a function of wind speed, wave-height to wave-period ratio, wave height, and period. Next, we consider the differential shift plotted vs the sea truth parameters, in a manner similar to that in M&C. However, here we define the differential shift as the measured peak Doppler shift minus all of the contributions discussed in Section 3, except the Bragg scatterer phase velocity.

Peak Doppler Shift vs Wind Speed

Figure 9 shows plots of Doppler shift vs wind speed, as was plotted in M&C, and with our theoretical fetch model overlayed. The coefficients used for the model curves are those derived in the

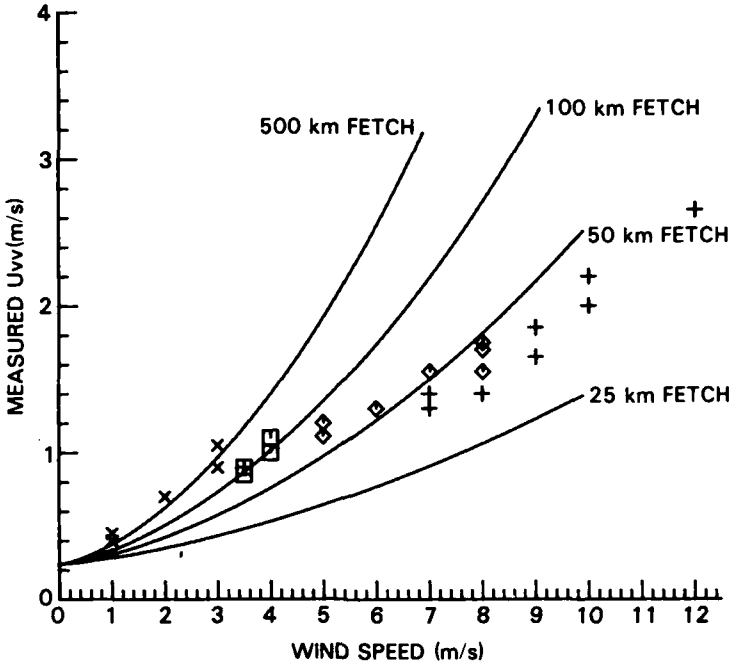

Fig. 9 — Radar peak Doppler shift vs wind speed with the same individual identifiers used for each data point as shown in the previous figures. The overlayed curves were calculated using Eqs. (9) and (10) in the three contributions to the Doppler shift given in Eqs. (3), (5), and (7), using the set of constants determined from the environmental data.

previous sections: $T_p = 1$, $H_p = 3$, $T_m = 0.8$, and $H_m = 5$. The expression relating the modeled Doppler shift V_d to wind speed V is determined by combining the three expressions given in Section 3, Eqs. (4a), (6), (8), and 24 cm/s for the Bragg scatterer phase velocity. Each of these are expressed in terms of wind speed through Eqs. (9) and (10), which relate wave height and period to wind speed through the modified Darbyshire model. The resulting expression is given by:

$$V_d = C_1 V^{1.5}/(1-C_2 V) + C_3 V^{2.5} + .02 V + .24 \quad (14)$$

in units of m/s. The $C_i = C_i(A,B,T_P,H_P,y)$ are in units of m/s. The $C_i = C_i(A,B,T_P,H_P,y)$ are given in the appendix. The choice of model as determined by the constants for the fetch variation all appear through the C_i coefficients.

Figure 9 looks similar to Fig. 7 because of the strong dependence of the orbital velocity contribution on the ratio H/T, as mentioned earlier. The same identifiers assigned to the curves earlier are maintained here for comparison. The three "X" data points of previous figures appear as five points now, since two pairs of points had the same height/period ratios and wind speeds, but have different peak Doppler shifts. Similar behavior is noted for the other points as well. The "+" data points lie within a tighter region in between the 25 and 50-km fetch curves in Fig. 9 than they did in Fig. 7, but within the same general area.

Note that the spread of the radar data is much narrower than the H/T data, with the "+" data lying above the 25-km fetch curve. This might be explained as follows: according to Eq. (12), the H/T ratio is a function of $V^{1.5}$, whereas Eq. (14) for the Doppler shift shows an added resonant term in the denominator. This term would cause a narrowing of this data for higher wind speeds, compared to the H/T data, as observed.

Note also that the lowest wind speeds achieve the fully developed fetch condition in general, while the higher wind speed data appear to group around a region of 50 km (or some other moderate value if one assumes that our constants are not the correct ones). Such a consistent fetch for the higher wind speeds could have been determined either by the wind direction and the land masses fixing a constant fetch in the experimental area (which was not specified), or by fetches determined by the movements of low pressure systems and associated fronts with their typical scale sizes.

Doppler Shift vs Wave-Height to Wave-Period Ratio

The second type of plot to consider is peak Doppler shift vs H/T. The expression for the Doppler shift in this case is:

$$V_d = \pi(H/T)/[1-C_4*(H/T)^{2/3}] + C_5*(H/T)^{5/3} + C_6*(H/T)^{2/3} + 0.24 \quad (15)$$

with the C_i coefficients again given in the appendix. The results of plotting this family of curves against the data are shown in Fig. 10 for the same constants used before. The first thing to note is that the theoretical curves are reversed in the sense of spread and show a smaller spread with increasing fetch for this case than for the other parameter comparisons. Whereas increasing H_p to greater than 1 causes a spread in the curves for the other parameter plots, in this case it causes a tightening. This tightening of the curves about the infinite fetch curve provides a poorer fit of the data than for the other curves, in fact. The infinite fetch curve fits the "X" sign data reasonably well, however.

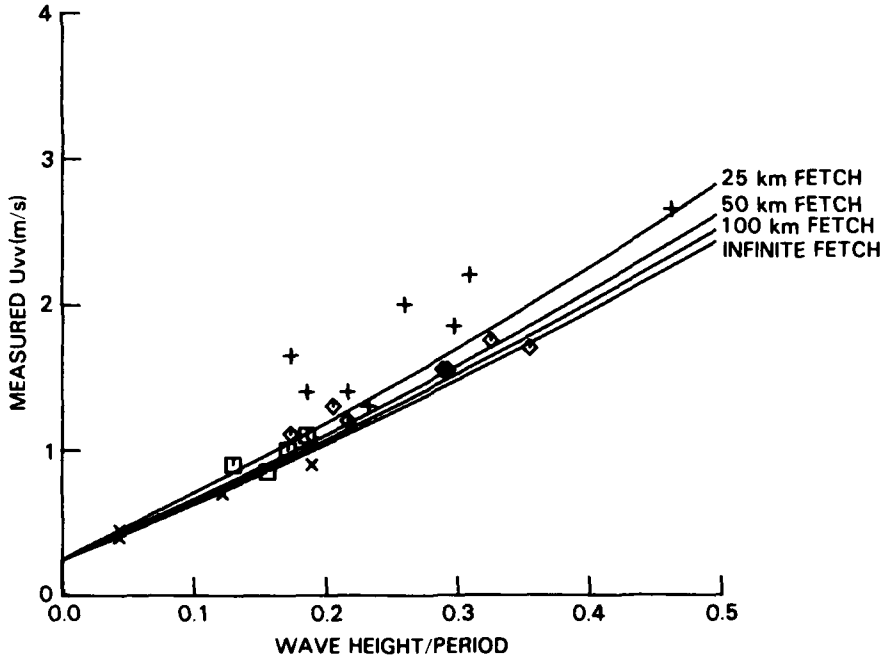

Fig. 10 — Radar peak Doppler shift vs the ratio of wave height over wave period are shown. Curves are overlayed using the same set of constants determined earlier. The spread of both the data and the theoretical curves is much smaller than it was in previous figures.

Doppler Shift vs Wave Height

The next data set plotted is that of peak Doppler shift vs wave height. In Fig. 11 we have plotted only the infinite fetch curve, and have also included Pidgeon's data for comparison, labeled with triangles. His data fall far below the M&C data and the model curves for all wave heights, which is not easily understood. In addition to the infinite fetch curve, we also plot the partial sums of the contributions to that curve to indicate their order of importance. This also allows one to test if perhaps one of the terms did not contribute strongly in Pidgeon's data, which does not seem to be the case. Pidgeon plotted the orbital wave velocity only (our dashed curve) and claimed a good fit. However, it is seen that none of the data points lie below the Bragg shift of 0.24 m/s, the minimum value that one could expect to find even for very light breezes. Thus, Pidgeon's data indicates the importance of including this contribution as well. Perhaps the reason for the poor fit of Pidgeon's data is the fact that his wave heights were determined from radar data, as discussed earlier, rather than from an actual *in situ* measurement.

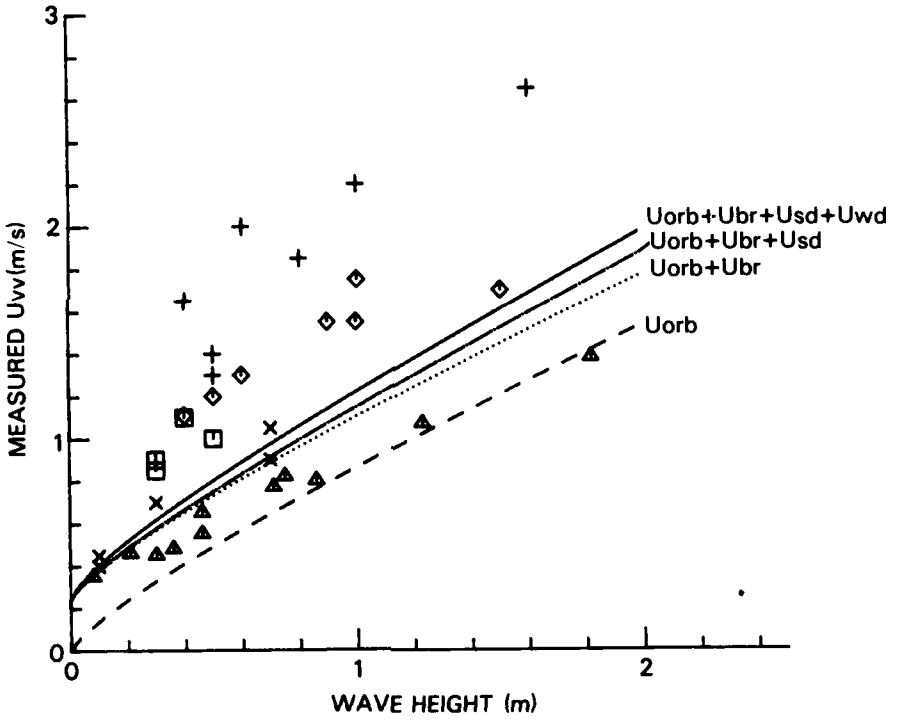

Fig. 11 — Doppler shift for vertically polarized sea scatter vs wave height is shown, similar to Pidgeon's reported results, and include Pidgeon's data marked by the triangle. The curves overlayed are for infinite fetch, and represent the partial sums of the contributions modeled in order of magnitude.

The curves for different fetches, with all contributions to the Doppler shift accounted for, are shown in Fig. 12, again for the same model constants. The sense of the spread of the data with fetch is correct again, and Pidgeon's data is seen to fall beyond the infinite fetch curve, again an indication of difficulty problems with his data.

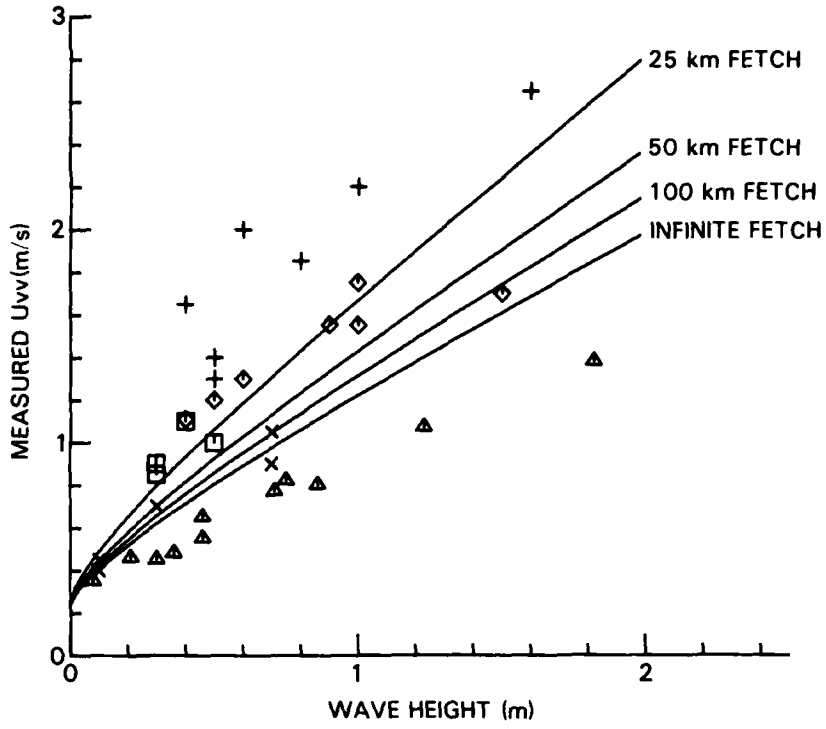

Fig. 12 — The data plotted are those of the previous figure, but with the total Doppler shift modeled by the curves and for the full set of fetches considered earlier. Note Pidgeon's data lie below the infinite fetch curve.

Peak Doppler Shift vs Wave Period

The final set of data plotted in this series is shown in Fig. 13, with the appropriate curves overlayed for the same set of constants as before. Although the "X"-, diamond-, and square-signed data are fit reasonably well by the corresponding fetch curves once again, the data represented by the "+" fall along higher fetch curves than before.

Discussion

The Doppler peak shift data show a more satisfactory comparison with the theoretical curves when plotted against the wind speed than when plotted against the wave parameters. However, all radar data show the correct trends in every case. One might argue that the wave data have a larger experimental measurement error than the wind data, and this causes the poorer fit. On the other hand, one could also argue that the Doppler shifts are effectively determined by the longest waves present, due to the shadowing of the shorter-wavelength smaller-wave height waves comprising the rest of the ocean wave spectrum. The rms wave height against which we plot includes all of these waves present in the spectrum, most of which may be shadowed. Hence, one should be comparing against the measured spectral amplitude of the peak of the spectrum, rather than an amplitude estimated from a measure of the rms wave height. This could improve the fits of both plots, Figs. 10 and 11, where both contain wave height as a parameter.

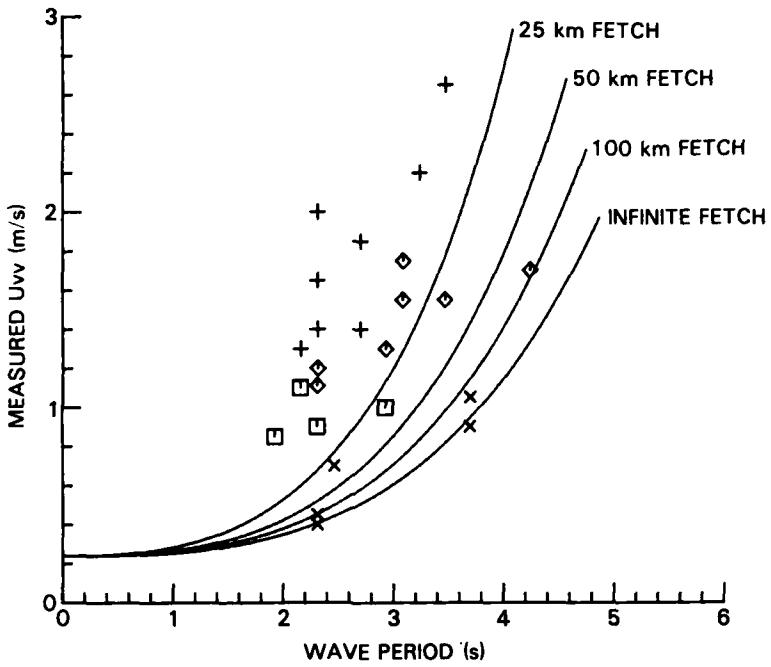

Fig. 13 — A plot of Doppler shift vs wave period, using the same set of constants determined earlier. Note the similar trends as in the previous figures.

7. DIFFERENTIAL VELOCITY VARIATION WITH ENVIRONMENTAL DATA

To compare our results with that of both Pidgeon and M&C, the differential velocity is now considered. This quantity is defined here as the measured peak Doppler shift minus the first three theoretical contributions defined in Section 3, with measured values of wind and wave parameters inserted into the modeled expressions, as before. The Bragg shift contribution, 0.24 m/s, is omitted, so that a perfect fit of the data to wind speed and the height-period ratio would be a line with zero slope, and y-intercept at 0.24 m/s. Pidgeon and M&C considered only the orbital wave velocity and wind drift velocity in their analysis, omitting the Stokes drift and Bragg scatterer phase velocity. In addition to plotting against wind speed, as in the above studies, we also plotted against the ratio of wave height to wave period.

As in Section 4, the three models given in Table 1 were used. The differential velocity vs wind speed are plotted in Fig. 14, exactly as in M&C, using the frequency of the peak of the spectrum and the expression for the orbital wave velocity given in Eq. 2. This differential velocity is then plotted vs the ratio of wave-height to average wave-period in Fig. 15. The data show an upward slope, as exhibited in M&C, whereas a correct model should produce a zero slope.

The same calculations are plotted in Fig. 16 and 17, but using the second model of Table 1. The slope of each curve is seen to diminish, so that the results are considered an improvement over the previous two figures, since the slope is approaching the expected zero value. Finally, we use the third model in the calculation of the differential velocity. The results are plotted in Figs. 18 and 19 vs wind speed and the height-period ratio, respectively, showing an even better fit to a zero-slope line.

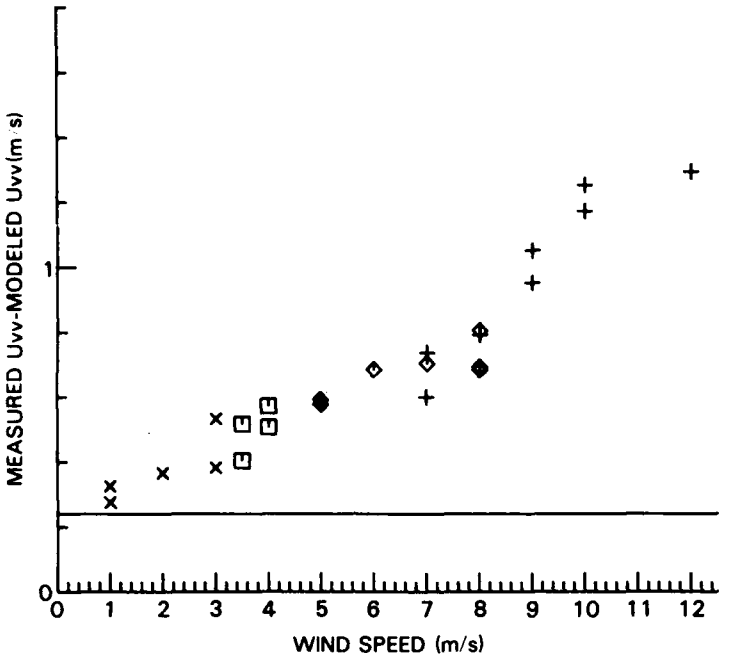

Fig. 14 — Differential velocity, the measured Doppler shift minus the modeled contributions, vs wind speed as reported by Mel'nichuk and Chernikov. The expressions of Model 1 were used here, as used by Mel'nichuk and Chernikov.

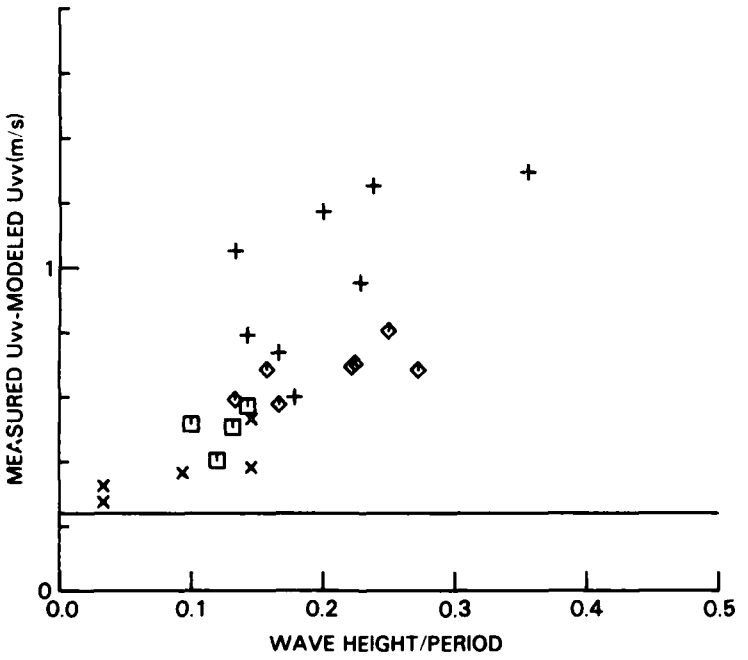

Fig. 15 — Differential velocity data reported by Mel'nichuk and Chernikov but vs the measured ratio of wave height over wave period using Model 1.

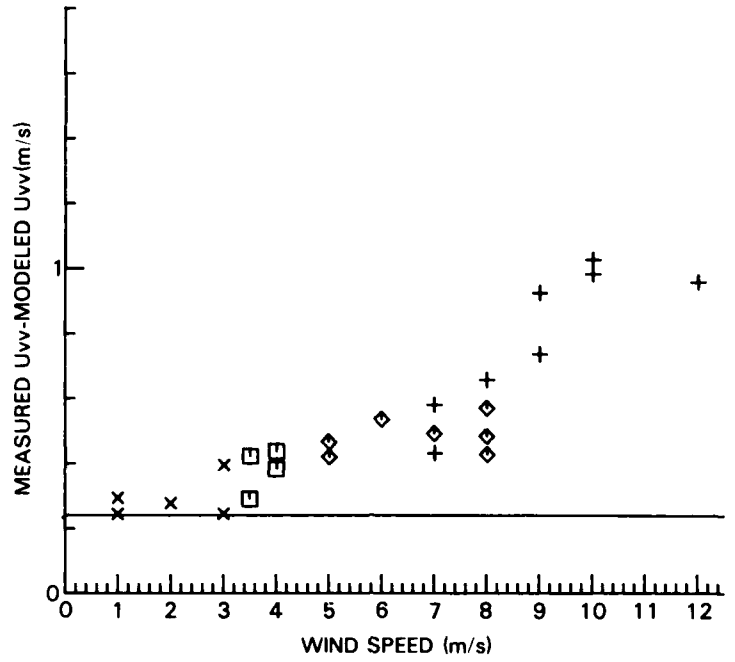

Fig. 16 — Differential velocity vs wind speed but using the second model of Table 1 as was done in Fig. 1b

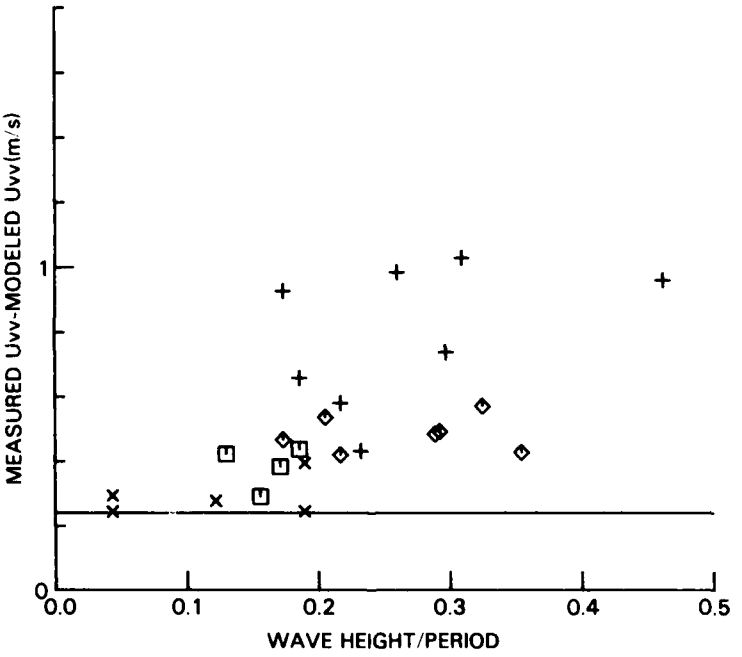

Fig. 17 — Differential velocity vs the wave height to period ratio but using Model 2, as in the previous figure

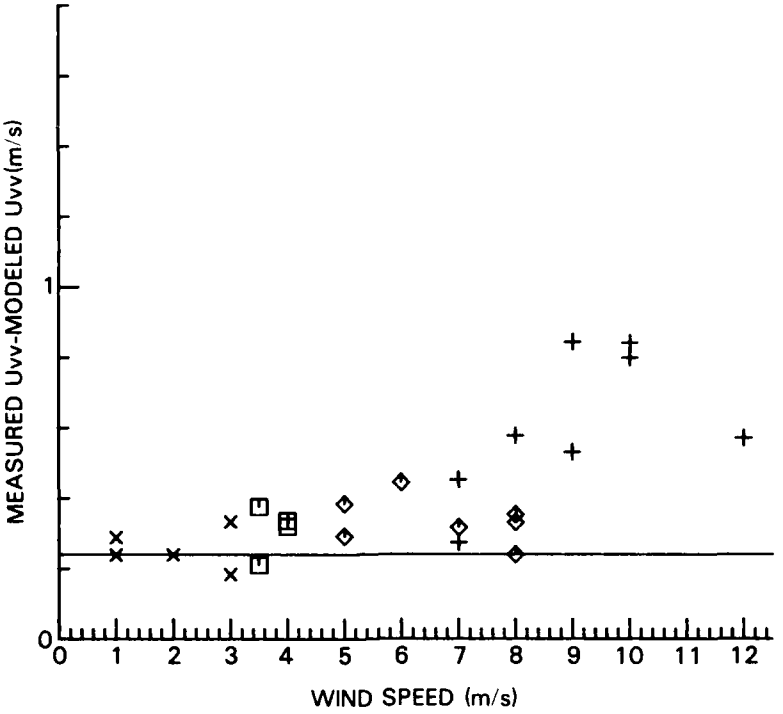

Fig. 18 — Differential velocity vs wind speed as shown in Fig. 16, but using Model 3, as was done in Fig. 1c

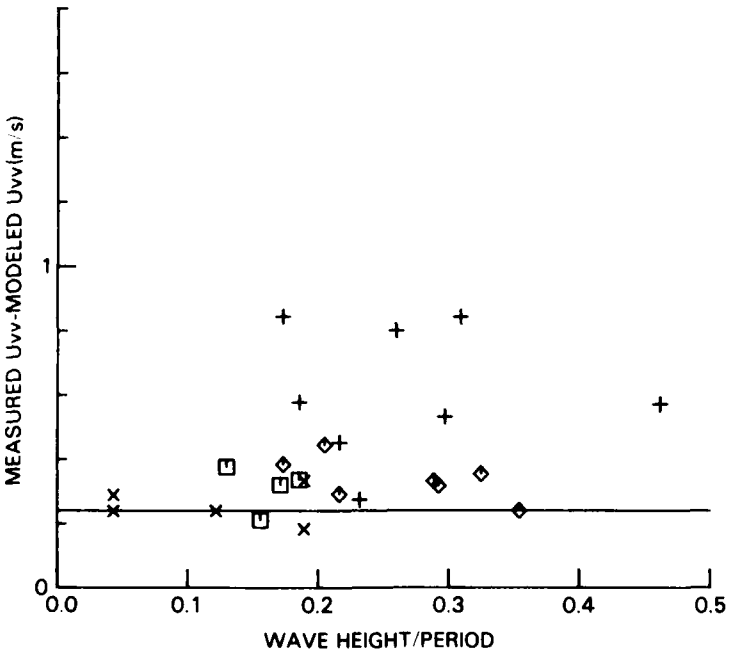

Fig. 19 — Differential velocity vs wave height for the choice of parameters of Model 3.

The improvement in the data fit occurs with use of the more exact expression for the orbital wave velocity and the peak frequency of the wave spectrum, in a manner similar to that in Section 4. The fit of the last pair of curves is quite good. Within experimental error, the data do fit a zero-slope line with y-intercept of .24 m/s, except for four of the short fetch data points that lie above the rest. These results can be considered another independent verification of the Doppler shift and scattering mechanisms being almost completely identified for the case of vertical polarization.

Results similar to this last pair are shown for cross-polarization and horizontal polarization in Figs. 20 and 21, and 22 and 23, respectively. The data show an upward bias, indicating that not all the scattering mechanisms have been identified for these two cases, in agreement with our conclusions in Section 4.

8. A SIMPLE MODEL FOR SPECTRAL PEAK DOPPLER SHIFT AND BANDWIDTH

Let us recapitulate. The consistency of each of the empirical fits of model curves through the different combinations of surface truth data in Figs. 6 and 7 allows one to implicitly scale these wave measurements with fetch. This is done utilizing our modified version of Darbyshire's model for wave-height dependence on fetch. Because fetch measurements were not available, the fetch values assigned to these curves cannot be taken as correct in an absolute sense, but only to within a scaling factor. There is a consistency in the labeled wave data points falling near curves defined by similar fetches of the model from one type of plot to the next. This suggests that variation in fetch is responsible for the spread in the surface truth data. This is, of course, based upon the original premise that duration was not a limiting factor in the wave development, assuming much less than 4 h were necessary for the wave periods measured, which is probably a reasonable assumption.

Next, the fit of the vertically polarized radar data to the radar model curves occurs for the same fetches as defined in Figs. 6 and 7. Thus, one can conclude that the spread in the radar data is also to fetch effects. An empirical model is thereby formulated for the prediction of the Doppler shift of the spectral peak. This model is equally uncertain as to the exact value of the fetch for each curve, as were the curves for the surface truth data.

We were not successful in identifying causes of the spectral peak Doppler shift for horizontal and cross-polarized cases. However, because of the relatively tight fit of the data for horizontally and cross-polarized Doppler shift plotted vs vertical Doppler shift in Figs. 4 and 5, these two parameters can be empirically scaled linearly to the vertically polarized Doppler shift predicted by the model, using slopes of 1.4 and 1.2, respectively.

Pidgeon's plots of Doppler spectral bandwidth vs peak Doppler shift allow us to relate the bandwidth to the sea surface parameters in a similar fashion. These results are, of course, valid only for the radar depression angles below 10 deg which were used for Pidgeon's experiments, but which therefore hold for the 2 deg or smaller depression angles in M&C. The slopes from Pidgeon's work are 1.143 for vertical polarization, and 0.571 for horizontal, with zero intercepts. Hence, the Doppler 3-dB bandwidth for vertical polarization will be 1.143 times the value of the peak Doppler shift. The much smaller factor for horizontal polarization indicates that the scatterers which produce the dominant contribution for this case have a much narrower spread in velocities. This might be expected to be the case for crest features on the very highest waves present, since all other crests are either shadowed or perhaps not as sharp edged if associated with smaller waves on the ocean surface.

Improvements to this model can be made by determining the exact scaling with fetch. This would be accomplished by making fetch measurements simultaneously with the other surface truth parameters measured in M&C. Secondly, the length of time for which the wind has blown should be accounted for in some way in addition to the fetch, particularly when considering data with longer wave periods than the 3 to 4 s in this study. As mentioned earlier, the duration limit is much less than 4 h for the waves

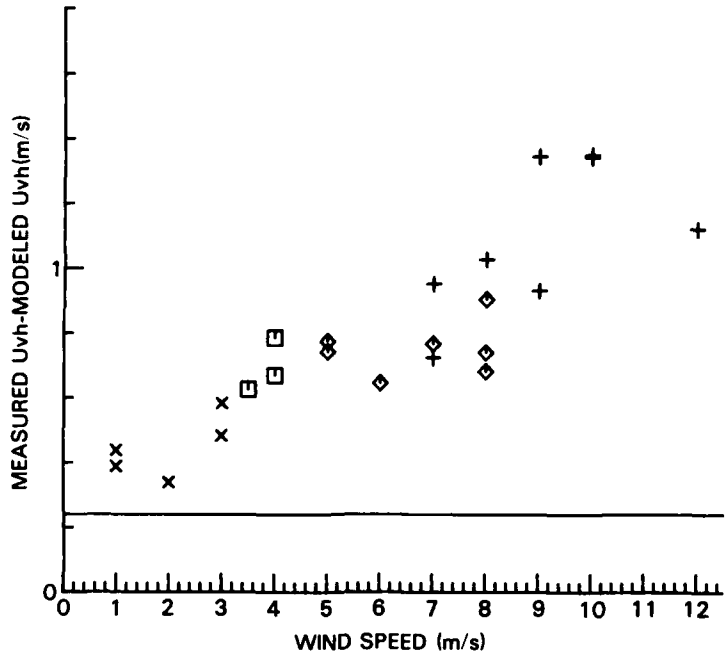

Fig. 20 — Differential velocity vs wind speed for the cross-polarized case, using Model 3.

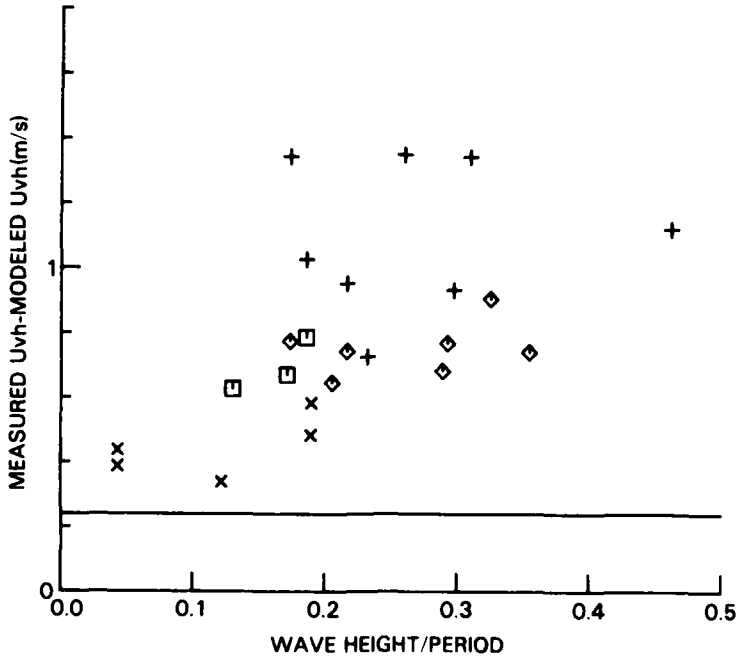

Fig. 21 — Differential velocity vs wave height for the cross-polarized case, using Model 3.

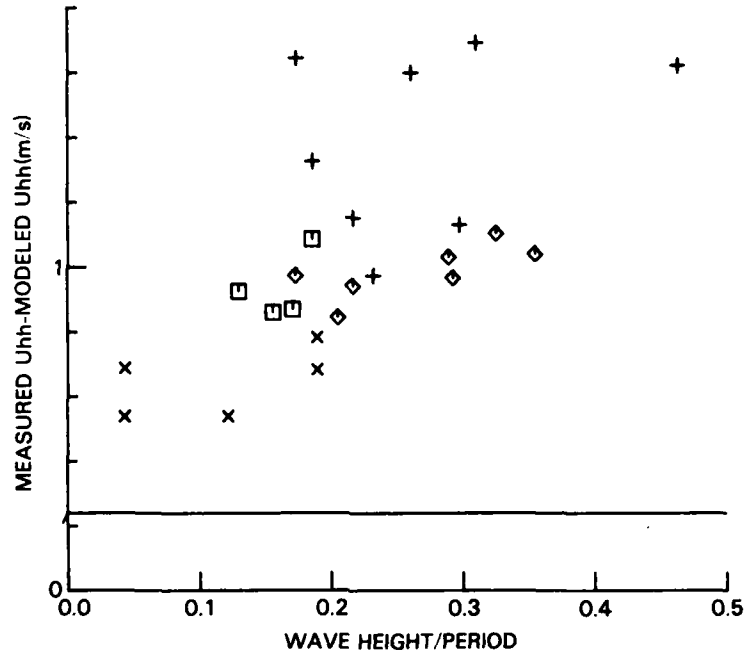

Fig. 22 — Differential velocity vs wind speed for the case of horizontal polarization, using Model 3.

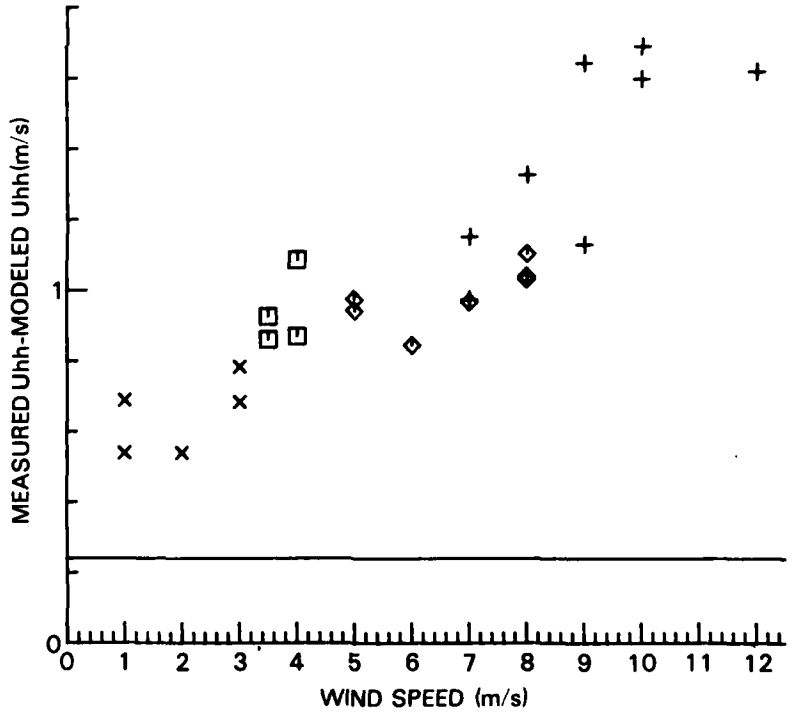

Fig. 23 — Differential velocity vs wave height for the case of horizontal polarization, using Model 3.

considered here, but longer wave periods require a longer duration which must be accounted for. Our model is presented to indicate the importance of including fetch as a parameter in the radar measurements, rather than as the final word on the subject at this time.

9 . DISCUSSION

From this Doppler spectral shift model, several conclusions may be drawn about radar scatter and small- and large-scale wave motion effects:

(a) The period of the peak of the ocean wave spectrum is the appropriate quantity to use in calculating Doppler shift contributions to the sea scatter Doppler spectrum for grazing angles less than two deg, and perhaps for even larger grazing angles. (A more rigorous treatment of shadowing would be required for modeling higher angles than is warranted here.) This implies that the largest components in the Doppler spectrum (those forming the spectral peak) are related to those ocean wave components with frequencies near the peak of the ocean wave spectrum, and that have the largest orbital wave velocities. (The wave spectrum was not reported in M&C, but most models for the wave spectrum scale as frequency to the minus-five, or wavelength to the third power, relating the highest wave components to those with longest wavelength.) This is primarily an effect of shadowing of the lower wave height, shorter wavelength waves by those high waves with frequencies near the peak of the ocean wave spectrum. In addition, however, this effect would also result if the small-scale Bragg scatterers were preferentially associated with the longest waves, even without shadowing present. This may in fact be the case for at least two reasons. The strongest interaction between the wind and waves might be expected to occur near the highest crests, where the airflow is subjected to the greatest distortion by the surface; small-scale wave breaking can be expected to occur near the largest crests.

(b) For vertically polarized X-band radar sea echo, the Doppler shift of the spectral peak is well-described by orbital wave motions, Stokes drift currents, wind drift currents of the large gravity waves, and the shift due to the phase velocity of the Bragg resonant capillary waves.

(c) For horizontally and cross-polarized returns, additional motions are required to explain the Doppler shifts which are observed to be larger than those for vertical polarization. When these shifts are plotted against the vertically polarized shifts for the same wind and wave conditions, they scale in a linear fashion, with slopes of 1.4 and 1.2 respectively. In addition, the observed scatter about this linear fit is uncorrelated with environmental parameters, and this scatter is very small in both cases. Hence, it appears that the scattering mechanisms for these two cases scale with wind and wave conditions in the same way as do those for vertical polarization.

These results provide several implications to remote sensing. Models for interpretation of SAR imagery at higher grazing angles sometimes differ over what velocity is to be used for the scatterer motion through the integration period. If the physics satisfying this model continue to hold as the depression angle approaches those used by SAR systems, then the orbital wave motion clearly dominates.

For purposes of inversion of SAR ocean wave imagery to obtain ocean wave parameters, the two-scale model alone is not sufficient for use in inversion algorithms for horizontal polarization. Other scattering contributions must be accounted for that have velocities in addition to, or which are greater than, those due to orbital wave motions. The contributions of specular scatterers for the near-grazing angle case may be important for vertical polarization, but only if their motions upon the large-scale waves are as described by the two-scale model. Wedge-type scatter due to near-breaking crest features may be important for horizontally polarized scatter (Lyzenga et al. [15]). Such features would be expected to provide a Doppler shift equal to the sum of the phase velocity of the dominant wave plus

that of the breaking wave crest feature. Because of the lack of data on breaking wave crest velocities and accelerations, these features have not been considered in the present model.

The possibility of applying low grazing angle, Doppler spectral peak shift measurements to remote sensing of the ocean surface is an interesting concept. The advantage is that a calibration of power is not required, since only relative backscatter amplitudes are important in establishing the Doppler spectral features. Because of the dominance of orbital wave and current motions on the Doppler shift of the sea scatter spectral peak, it appears that Doppler spectral peak measurements can provide information about the large-scale structure of the waves. This is in contrast to the sea surface radar cross section (RCS), which is known to depend on the small-scale wave structure, and is a strong function of the wind stress (see, for example, Liu and Ross [14]). With a sharp drop in wind speed, and therefore stress, the RCS decreases almost instantaneously, since the probability of occurrence of small-scale waves decreases accordingly.

Given a measurement of the wind speed, wind drift currents can be estimated and subtracted from the peak shift, along with the Bragg shift. Using the remainder, an estimate of the wave height to wavelength ratio can be made by using the equations developed in the text. A shipboard radar operating in a high-resolution mode can be used to estimate the spacing of the dominant waves (Trizna and Porter [16]). Combining these two estimates, the dominant wave height could be retrieved.

Wind stress is of interest to climatologists, wave forecasters, and upper ocean modelers, and is related to the wind speed V, measured at altitude Z, according to:

$$\tau = \rho\ Cd(Z)\ V(Z)^2$$

where ρ is the density of air, and $Cd(Z)$ is the drag coefficient measured at the same altitude as the wind. Recent work by Donelan [17] suggests that the spread among the values of the drag coefficient observed in different air-sea interaction experiments may be due to different large-scale wave conditions, rather than to experimental error. Thus, Cd may be influenced by the ocean wave spectrum, or at a minimum, by the dominant wave length and height. It would appear that if the near-grazing angle sea surface RCS is dependent upon the wind stress, then measurements of RCS and Doppler spectral peak shift made by a shipboard radar could provide all of the information necessary for a measure of wind stress, including the large-scale wave effects suggested by Donelan.

10. ACKNOWLEDGMENT

The author acknowledges suggestions made by Dr. Lewis Wetzel which added to the clarity of the presentation of the several ideas discussed in the report.

11. REFERENCES

1. V.W. Pidgeon, "Doppler Dependence of Radar Sea Return," *J. Geophys. Res.* **73**, 1333-1341 (1968).

2. Y.U. Mel'nichuk and A.A. Chernikov, "Spectra of Radar Signals from Sea Surface for Different Polarizations," Izvestia, *Atmos. & Oceanic Phys.* **7**, 17-24 (1971).

3. G.R. Valenzuela, "The Effect of Capillarity and Resonant Interactions on the Second-order Doppler Spectrum of Sea Echo," *JGR* **79**, 5031-5037 (1974).

4. B.L. Hicks, N. Knable, J.J. Kovaly, G.S. Newell, J.P. Ruina, and C.W Sherwin, "The Spectrum of X-band Radiation Backscattered from the Sea Surface," *JGR* **65**, 825-837 (1960).

5. J.R. Duncan, W.C. Keller, and J.W. Wright, "Fetch and Wind Speed Dependence of Doppler Spectra," *Radio Sci.* **9**, 809-819 (1974).

6. J.W. Wright, "A New Model for Sea Clutter," *IEEE Trans. Anten. & Prop.* **AP-16**, 217-223 (1968).

7. J. Darbyshire, "Further Investigations of Wind-driven Perturbation," *Coll.: Wind Waves* (IL Press, 1962).

8. O.M. Phillips, *The Dynamics of the Upper Ocean*, 2nd ed. (Cambridge University Press, 1977).

9. D.D. Crombie, "Doppler Spectrum of Sea Echo at 13.56 Mc/s," *Nature* **175**, 681-682 (1955).

10. T.R. Mee, Cornell Aeron. Lab., Cornell Univ. Rept, RG-1623-P-1, 1963.

11. B. Kinsman, *Wind Waves* (Prentice-Hall, Englewood Cliffs, NJ, 1965).

12. E.B. Kraus, *Atmosphere-Ocean Interaction* (Clarendon Press, Oxford, 1972).

13. H.U. Sverdrup and W.H. Munk, "Wind, Sea, and Swell: Theory of Relations for Forecasting," U.S. Navy Hydrographic Office Pub. No. 601 (1947).

14. P.C. Liu and D.B. Ross, "Airborne Measurements of Wave Growth for Stable and Unstable Atmospheres in Lake Michigan," *J. Phys. Ocean* **10**, 1842-1853 (1980).

15. D.R. Lyzenga, A.L. Maffett, and R.A. Shuchman, "The Contribution of Wedge Scattering to the Radar Cross Section of the Ocean Surface," *IEEE Trans. Geoscience and Remote Sensing* **GE-21**, 502-505 (1983).

16. D.B. Trizna and D.L. Porter, "A Technique for Estimating RMS Waveheight and Dominant Wave Period Using a Coherent Shipboard Radar," *Conference Record*, Oceans '84, Sept. 10-12, 1984, Washington, D.C., pp. 134-137.

17. M.A. Donelan, "The Dependence of the Aerodynamic Drag Coefficient on Wave Parameters," Proceedings of the First International Conference on Meteorology and Air/Sea Interaction of the Coastal Zone," Am. Met. Soc., Boston, MA, 1982.

Appendix
MODEL COEFFICIENTS

The coefficients in Eqs. (14) and (15) are derived by using the expressions given in Eqs. (9), (10), and (13) in terms of the model parameters H_m, H_p, T_m, and T_p. One can rewrite these latter equations more simply as:

$$H = A\ V_w^2 \tag{A1}$$

$$T = B\ V_w^{1/2} \tag{A2}$$

$$H/T = (A/B)\ V_w^{5/2}. \tag{A3}$$

Then, substituting these in Eqs. (4a), (6), and (8), one gets:

$$C_1 = \pi(A/B) \tag{A4}$$

$$C_2 = (2\pi/g)(A/B^2) \tag{A5}$$

$$C_3 = (\pi^3/g)(A^2/B^3) \tag{A6}$$

to be used in Eq. (14).

If one inverts Eq. (A3) to solve for V_w, one gets

$$V_w = (B/A)^{2/3}(H/T)^{2/3} \tag{A7}$$

which can be substituted into Eq. (14) to give the peak Doppler shift in terms of H/T. The coefficients can be expressed in terms of C_1, C_2, and C_3 as follows:

$$C_4 = C2*(B/A)^{2/3} \tag{A8}$$

$$C_5 = C3*(B/A)^{5/3} \tag{A9}$$

$$C_6 = .02*(B/A)^{2/3}. \tag{A10}$$

These coefficients are used in Eq. (15) for the peak Doppler shift as a function of H/T.

☆ U.S. Government Printing Office : 1985 - 530-039/40036

END

FILMED

12-85

DTIC